

Hydrothermal crystallization of uranyl coordination polymers involving an imidazolium dicarboxylate ligand: effect of pH on the nuclearity of uranyl-centered sub-units.

Nicolas P. Martin,^a Clément Falaise,^a Christophe Volkringer,^{a,b} Natacha Henry,^a Pierre Farger,^c Camille Falk,^c Emilie Delahaye,^c Pierre Rabu,^c Thierry Loiseau.^{a,*}

Contribution from

^a*Unité de Catalyse et Chimie du Solide (UCCS) – UMR CNRS 8181, Université de Lille, ENSCL, Bat C7, BP 90108, 59652 Villeneuve d'Ascq, France.*

^b*Institut Universitaire de France, 1 rue Descartes, 75231 Paris Cedex 05.*

^c*IPCMS UMR7504 CNRS-UNISTRA, Département de Chimie des Matériaux Inorganiques, 23, rue du Loess, BP43, Strasbourg cedex 2, France.*

* To whom correspondence should be addressed. E-mail: thierry.loiseau@ensc-lille.fr. Phone: (33) 3 20 434 434, Fax: (33) 3 20 43 48 95.

SUPPLEMENTARY INFORMATION

To be submitted to Inorg. Chem.

Version May 20, 2016.

Revised version june 16, 2016.

Revised version july 22, 2016.

Figures

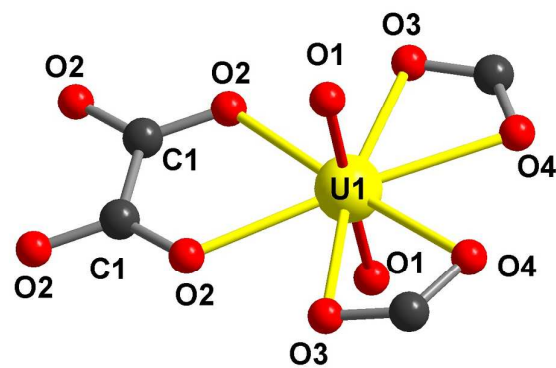


Figure S1a: View of the coordination of uranyl center U1 in $(\text{UO}_2)_2(\text{imdc})_2(\text{ox}) \cdot 3\text{H}_2\text{O}$ (**1**).

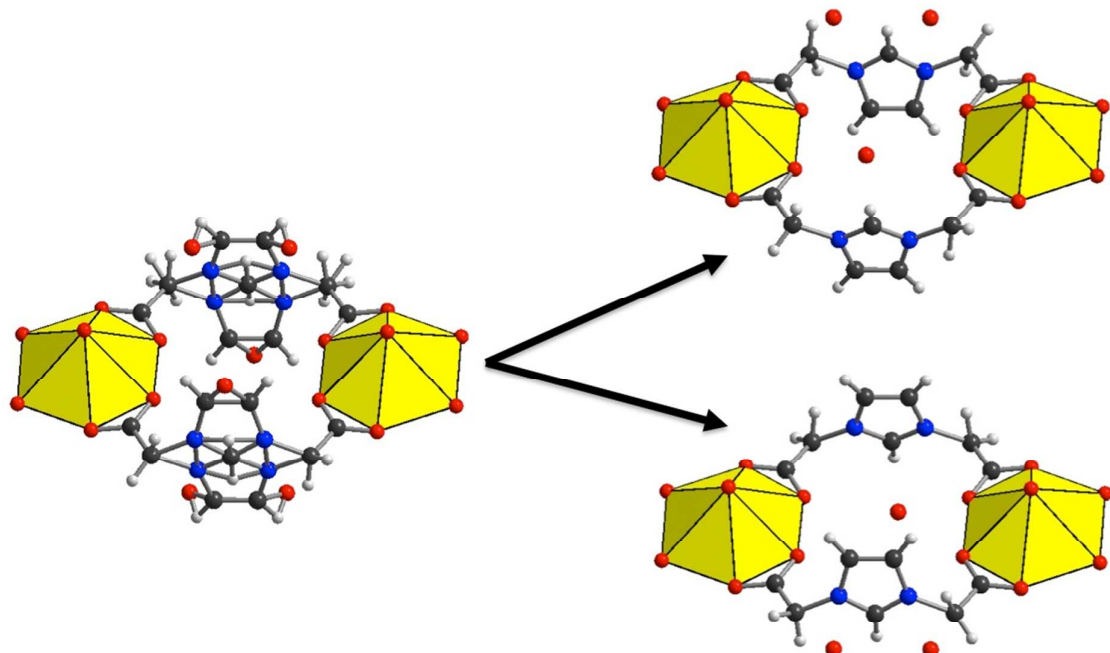


Figure S1b: Detailed view of the disorder of the imidazol ring and water molecules in $(\text{UO}_2)_2(\text{imdc})_2(\text{ox}) \cdot 3\text{H}_2\text{O}$ (**1**).

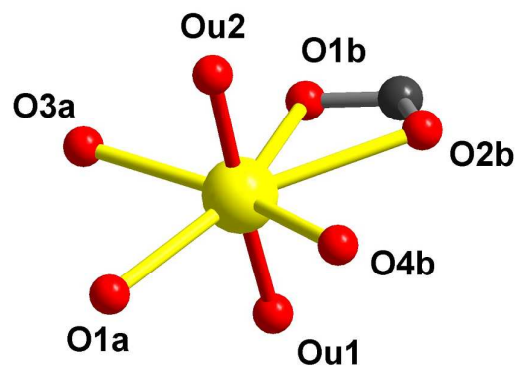


Figure S1c: View of the coordination of uranyl center U1 in $(\text{UO}_2)(imdc)_2$ (**2**).

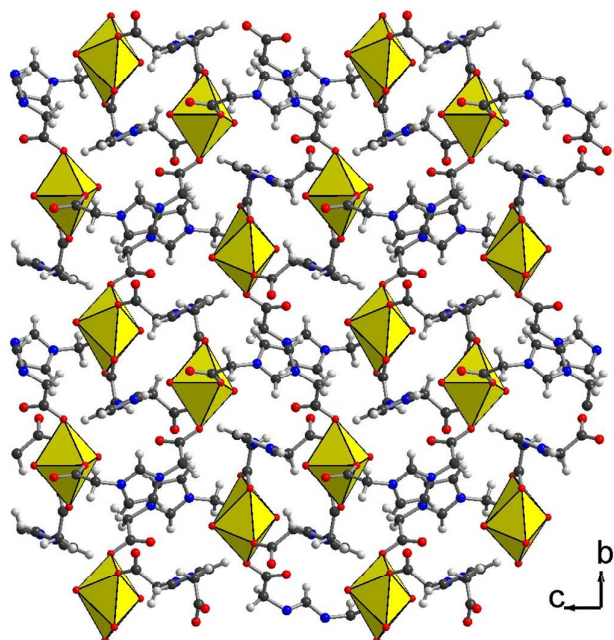


Figure S1d: Representation of a layer in the (b,c) plane in $(\text{UO}_2(imdc)}_2$ (**2**).

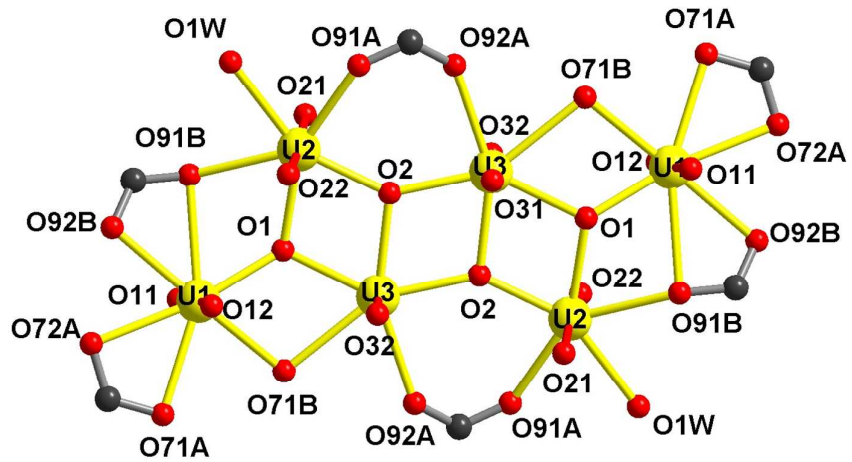


Figure S1e: View of the coordination of uranyl centers U1, U2 & U3 in $(\text{UO}_2)_3\text{O}_2(\text{H}_2\text{O})(\text{imdc}) \cdot \text{H}_2\text{O}$ (3).

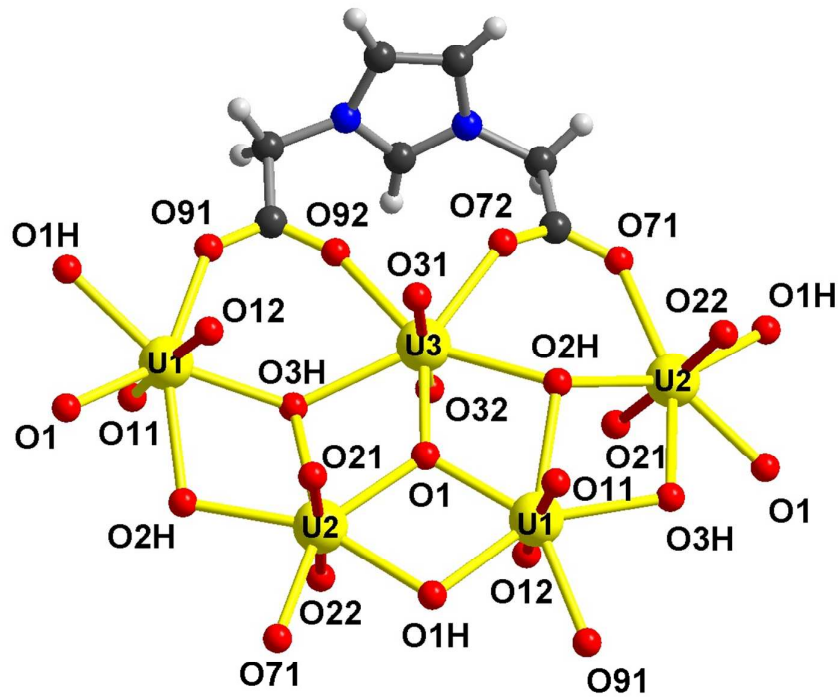


Figure S1f: view of the coordination of uranyl centers U1, U2 & U3 in $(\text{UO}_2)_3\text{O}(\text{OH})_3(\text{imdc}) \cdot 2\text{H}_2\text{O}$ (**4**).

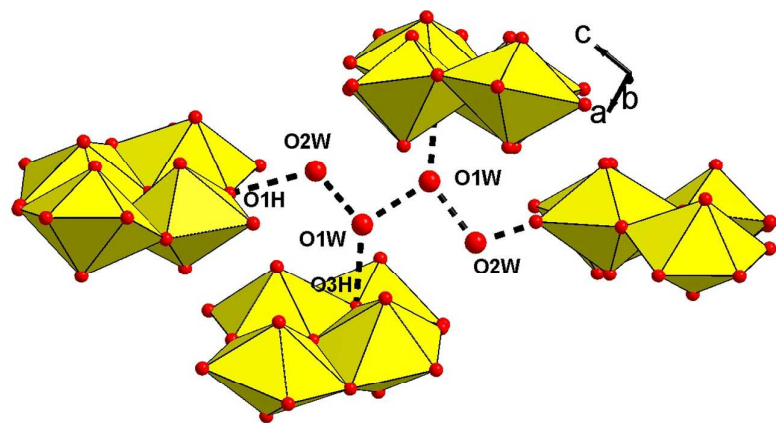


Figure S1g: View of the hydrogen bond scheme in $(\text{UO}_2)_3\text{O}(\text{OH})_3(\text{imdc}) \cdot 2\text{H}_2\text{O}$ (**4**)

XRD powder patterns

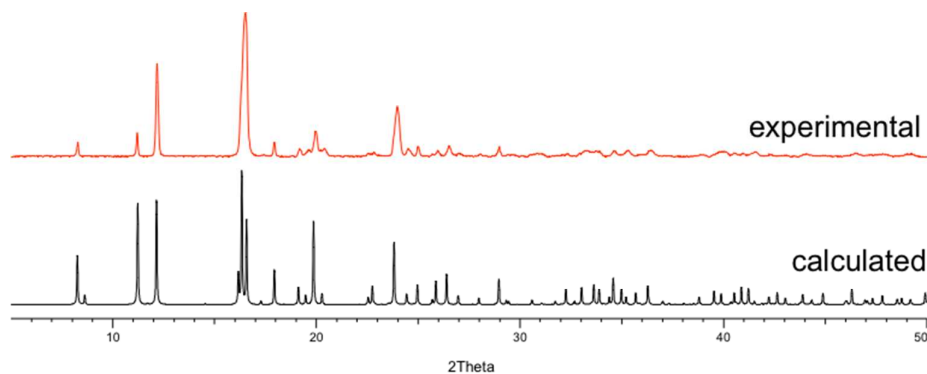


Figure S2a: Comparison between the calculated (black line) and experimental (red line) XRD patterns of $(\text{UO}_2)_2(\text{imdc})_2(\text{ox}) \cdot 3\text{H}_2\text{O}$ (**1**) – Copper radiation.

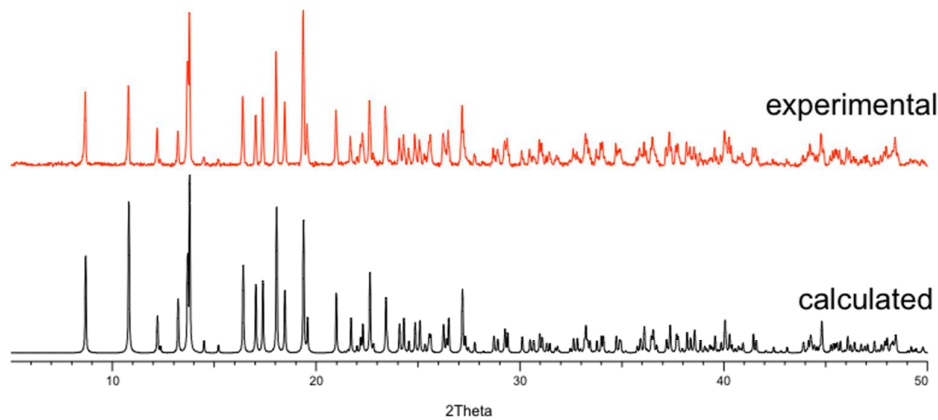


Figure S2b: Comparison between the calculated (black line) and experimental (red line) XRD patterns of $\text{UO}_2(\text{imdc})_2$ (**2**) – Copper radiation.

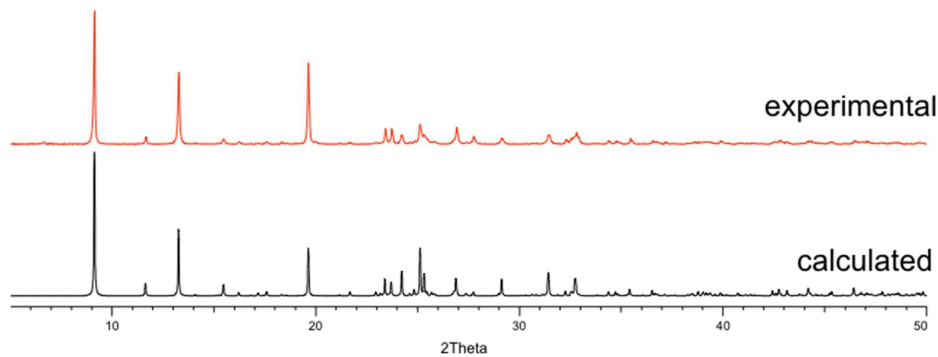


Figure S2c: Comparison between the calculated (black line) and experimental (red line) XRD patterns of $(\text{UO}_2)_3\text{O}(\text{OH})_3(\text{imdc}) \cdot 2\text{H}_2\text{O}$ (**4**) – Copper radiation.

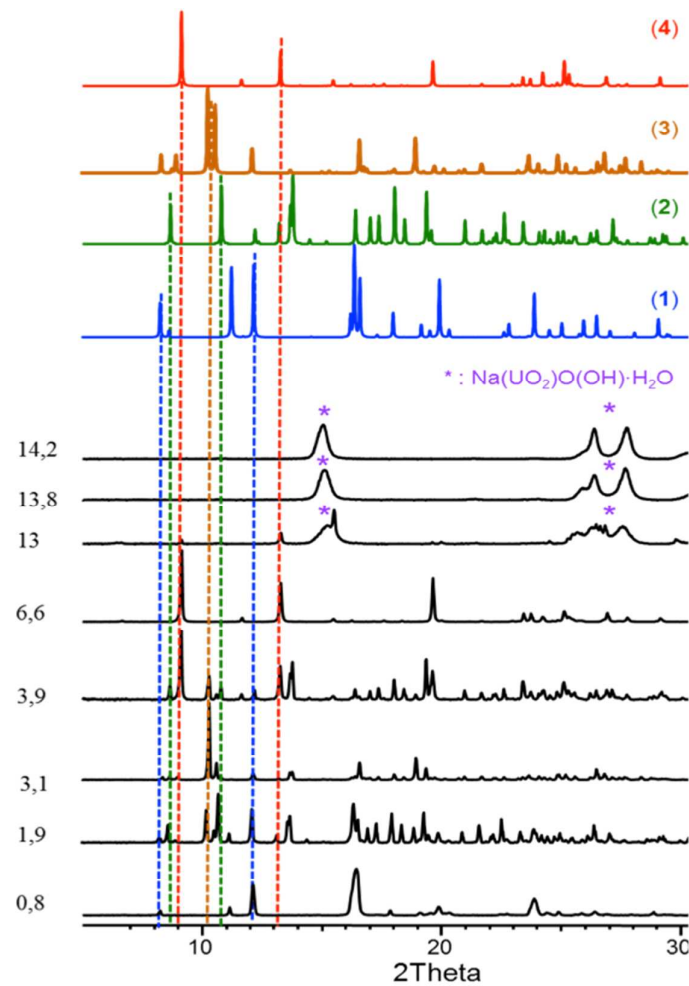


Figure S3: Evolution of the powder XRD patterns of compounds **1-4** & $\text{Na}(\text{UO}_2)\text{O}(\text{OH})\cdot\text{H}_2\text{O}$, as a function of reaction pH.

Thermal analysis. The thermogravimetric experiments have been carried out on a thermoanalyzer TGA 92 SETARAM under air atmosphere with a heating rate of $5^{\circ}\text{C}.\text{min}^{-1}$ from room temperature up to 800°C .

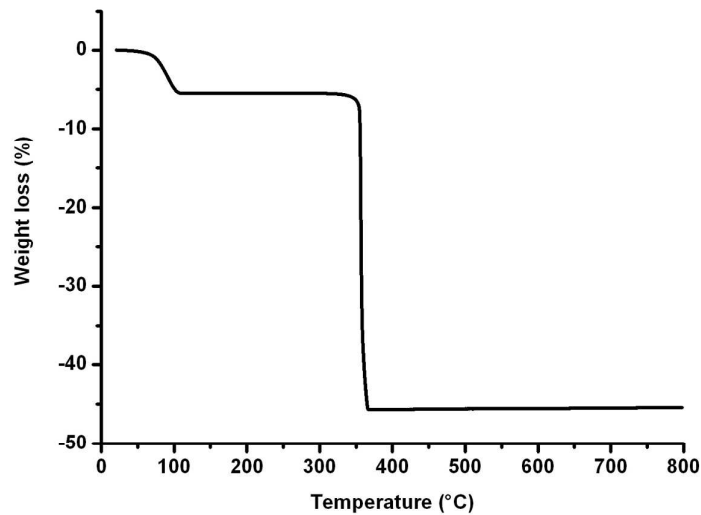


Figure S4a: Thermogravimetric curve of the compound $(\text{UO}_2)_2(\text{imdc})_2(\text{ox}) \cdot 3\text{H}_2\text{O}$ (**1**) under air atmosphere (heating rate $5^{\circ}\text{C}.\text{min}^{-1}$).

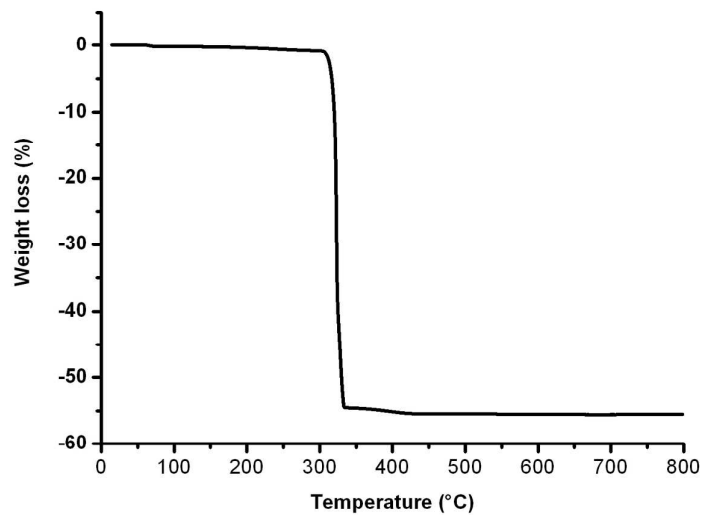


Figure S4b: Thermogravimetric curve of the compound $\text{UO}_2(\text{imdc})_2$ (**2**) under air atmosphere (heating rate $5^{\circ}\text{C}.\text{min}^{-1}$).

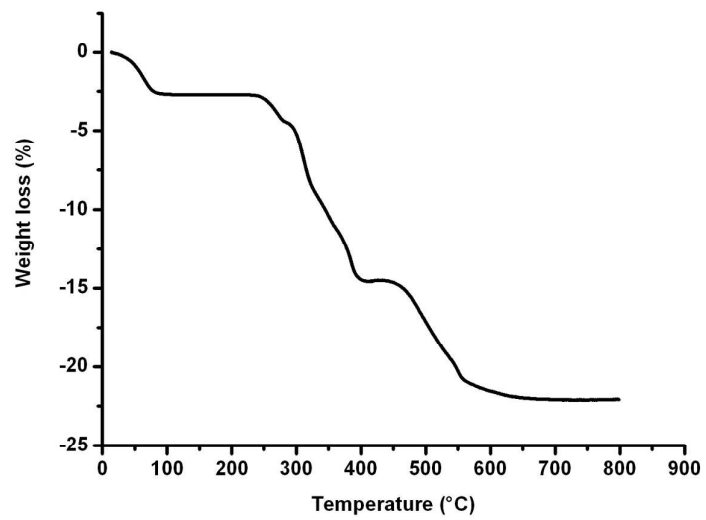


Figure S4c: Thermogravimetric curve of the compound $(\text{UO}_2)_3\text{O}(\text{OH})_3(\text{imdc}) \cdot 2\text{H}_2\text{O}$ (**4**) under air atmosphere (heating rate $5^\circ\text{C} \cdot \text{min}^{-1}$).

Infrared spectroscopy.

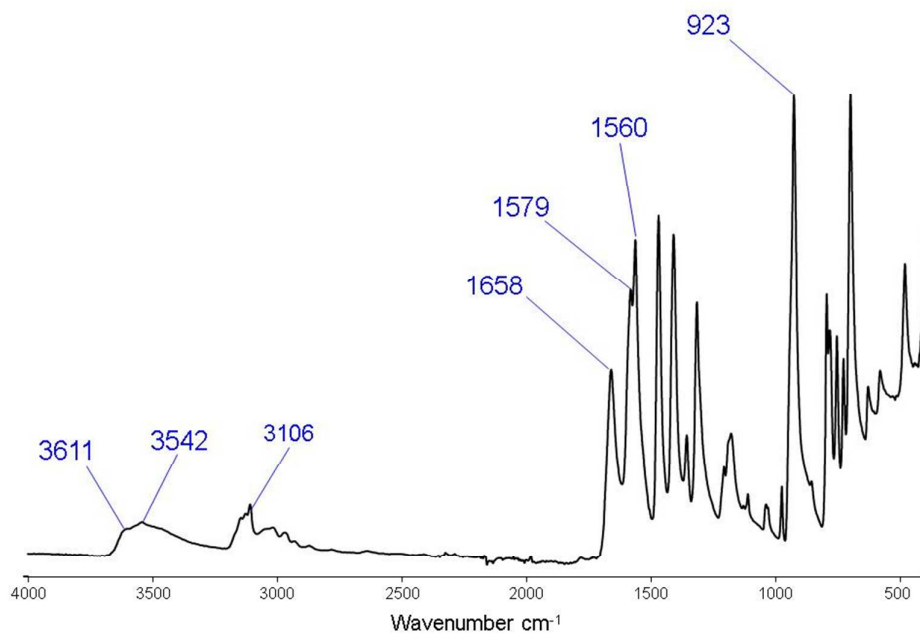


Figure S5a: Infrared spectra of $(\text{UO}_2)_2(\text{imdc})_2(\text{ox}) \cdot 3\text{H}_2\text{O}$ (**1**) collected at room temperature.

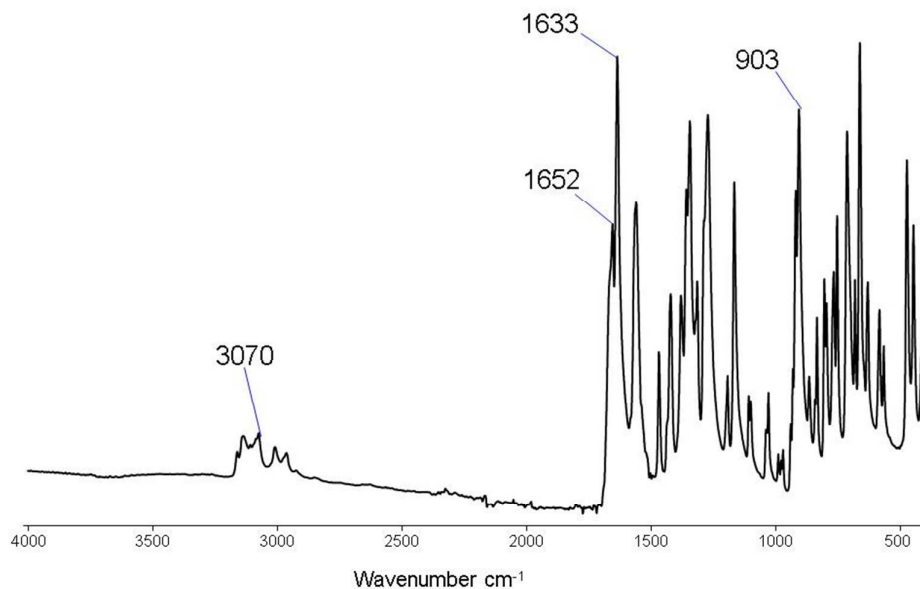


Figure S5b: Infrared spectra of $\text{UO}_2(\text{imdc})_2$ (**2**) collected at room temperature.

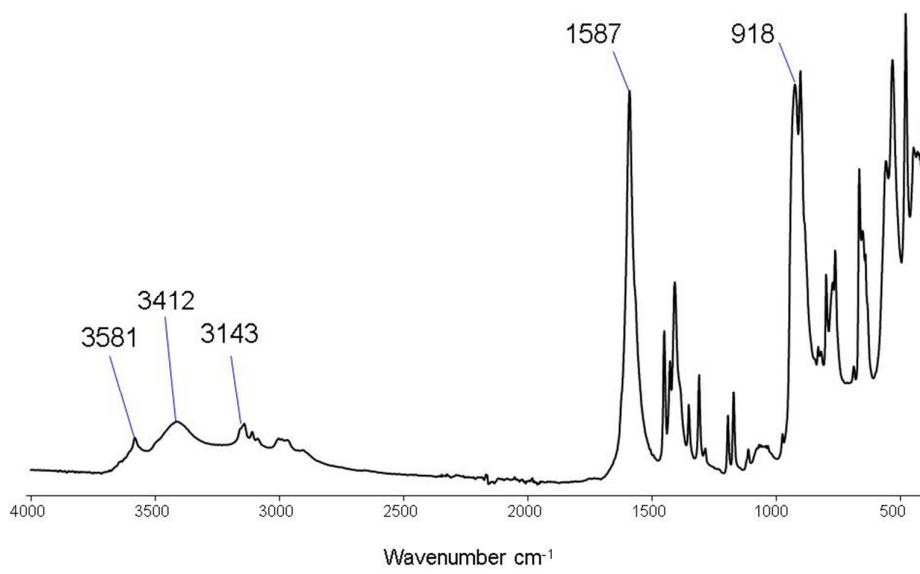


Figure S5c: Infrared spectra of $(\text{UO}_2)_3\text{O}(\text{OH})_3(\text{imdc}) \cdot 2\text{H}_2\text{O}$ (**4**) collected at room temperature.

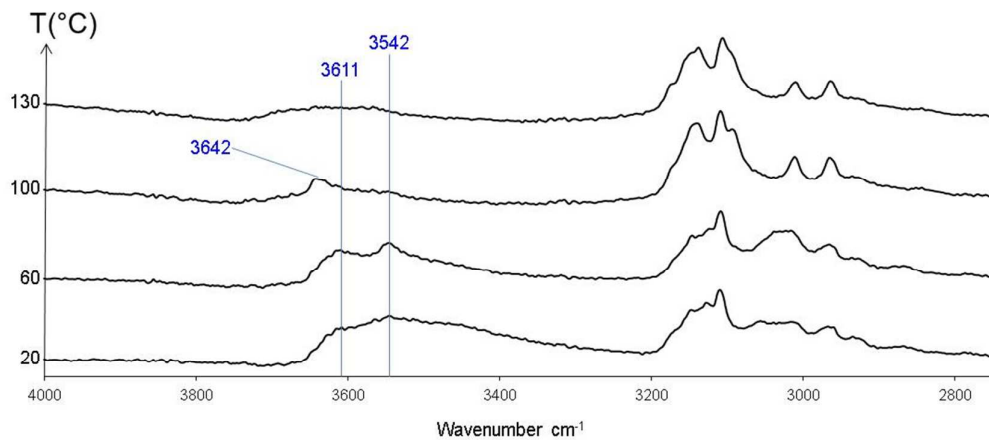


Figure S5d: Evolution of the *in situ* IR spectra of $(\text{UO}_2)_2(\text{imdc})_2(\text{ox}) \cdot 3\text{H}_2\text{O}$ (**1**) between 20-130°C in the range 4000-2750 cm⁻¹.

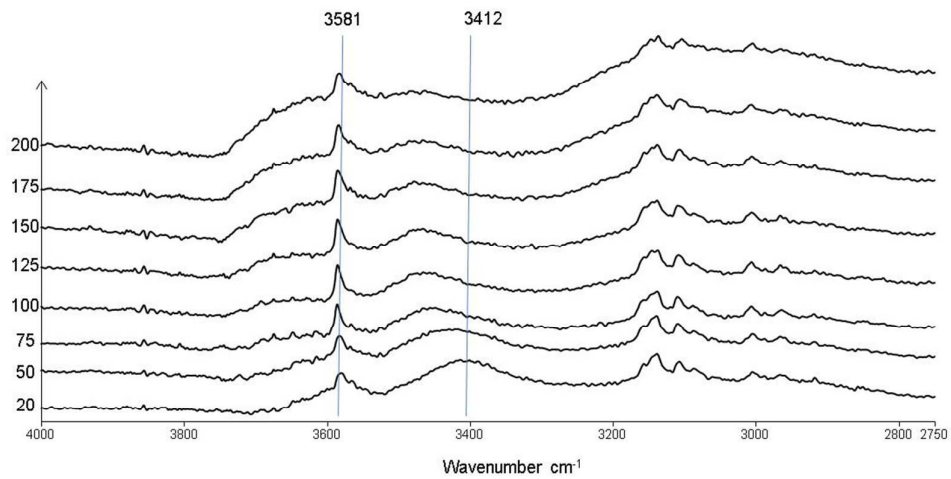


Figure S5e: Evolution of the in situ IR spectra of $(\text{UO}_2)_3\text{O}(\text{OH})_3(\text{imdc}) \cdot 2\text{H}_2\text{O}$ (**4**) between 20-200°C in the range 4000-2750 cm^{-1} .

Table S2: Comparison of U=O bond distance calculated from the position of $\nu_{\text{asym}(\text{U=O})}$ vibration and the crystal structure data.

| Phase | $\nu_{\text{asym}(\text{U=O})}$ | Distance U=O | |
|-------|---------------------------------|--------------|--------|
| | | Exp. | Calc.* |
| 1 | 923 | 1.73-1.77 | 1.76 |
| 2 | 903 | 1.79-1.80 | 1.78 |
| 3 | 918 | 1.76-1.78 | 1.77 |

*after J.R. Bartlett, R.P. Cooney, J. Mol. Struct. 193 (1989) 295.

Table S3: Positions of the bands (in nm – top – and cm⁻¹ – bottom –) in the fluorescence spectra of compounds **1**, **2** & **4**.

| Sample | | | | | |
|----------|----------------|------------------|-------------------|------------------|------------------|
| 1 | 490.5 20408 | 511 19569 | 533 18762 | 558 17921 | 585 17094 |
| 2 | 494 20243 | 514.5 19455 | 537.5 18622 | 561.5 17825 | 589 16978 |
| 4 | / | 520 (s) 19231 | 535(max) 18692 | 558 (s) 17921 | 585 (s) 17094 |

(s) shoulder